

COMBUSTION SYNTHESIS AND PHOTOLUMINESCENCE PROPERTIES OF NOVEL Eu^{3+} ION DOPED MAGNESIUM YTTRIUM BORATE PHOSPHOR

K.A. KOPARKAR, N. S. BAJAJ, S. K. OMANWAR

Department of Physics, Sant Gadge Baba Amravati University, Amravati-444 602, (INDIA)
E-mail: kakoparkar@gmail.com, Email: nsb.0208@yahoo.com, omanwar@sgbau.ac.in

Received April 27, 2014

The novel $\text{MgY}_{(2-x)}\text{B}_2\text{O}_7:\text{Eu}^{3+}$ prepared by solution combustion synthesis. The as-prepared samples were characterized by X-ray diffraction (XRD), and scanning electron microscope (SEM) for structural and morphological studies. The complete agreement of XRD with standard ICDD data confirms the formation of required phase. The optical studies were carried out by photoluminescence (PL) spectroscopy. The PL spectra reveal that the red emission (${}^3\text{D}_0 \rightarrow {}^7\text{F}_2$) was more intense than the orange emission (${}^5\text{D}_0 \rightarrow {}^7\text{F}_1$). The CIE chromaticity colour coordinates were calculated.

Key words: Optical material; phosphors; $\text{MgY}_{(2-x)}\text{B}_2\text{O}_7:\text{Eu}^{3+}$; CIE diagram.

1. INTRODUCTION

Alkaline metal yttrium borate host doped with *Rare-Earth* (RE) ions more demand in the field of luminescence, because they have easy to synthesis, high color purities and low thermal degradation [1]. The yttrium based phosphors is an excellent host for luminescent materials. Yttrium based compounds possess excellent optical properties. Recently, compound of alkaline with yttrium based family seem to be promising for high luminescent efficiency and good thermal stability [2]. In addition, borates have exceptional optical damage threshold and able to withstand the harsh condition in vacuum discharge lamps or screens. Because of excellent chemistry and thermal stabilization, facile synthesis and cheap raw material, these materials have been extensively applied in lamps and displays applications. Variety of borate host materials doped with rare earth and other ions have been reported for variety of applications [3-5].

It is well known that rare earth doped yttrium based materials have comparatively good luminescence properties, such as $\text{Li}_6\text{Y}(\text{BO}_3)_3:\text{Eu}^{3+}$ [6], $\text{Y}_3\text{Al}_5\text{O}_{12}:\text{Dy}^{3+}$, Bi^{3+} [7], $\text{YBO}_3:\text{Eu}^{3+}$ [8], $\text{Sr}_3\text{Y}(\text{PO}_4)_3:\text{Eu}^{3+}$ [9], etc.

In the present paper, we have reported the preparation and characterization of $\text{MgY}_{(2-x)}\text{B}_2\text{O}_7 \cdot x\text{Eu}^{3+}$ phosphor synthesized through solution combustion method. Further, PL spectra of the $\text{MgY}_{(2-x)}\text{B}_2\text{O}_7 \cdot x\text{Eu}^{3+}$ phosphors was investigated in detail.

2. EXPERIMENTAL

The $\text{MgY}_{(2-x)}\text{B}_2\text{O}_7 \cdot x\text{Eu}^{3+}$ samples were first time prepared by a solution combustion synthesis. The method is based on the exothermic reaction between the urea as a fuel and ammonium nitrate as a oxidizer. The detailed description of the method was reported in our earlier work [10, 11]. All the AR grade ingredients used in solution combustion synthesis such as $\text{Mg}(\text{NO}_3)_2$, $\text{Y}(\text{NO}_3)_3$, H_3BO_3 , $\text{CO}(\text{NH}_2)_2$, NH_4NO_3 and $\text{Eu}(\text{NO}_3)_3$ mixed thoroughly in agate mortar, so that the paste was formed. The stoichiometric amounts of the ingredients were thoroughly mixed in an Agate Mortar, then adding little amount of double distilled water to get an aqueous homogeneous solution. This solution was then transferred into a china basin and slowly heated at lower temperature of 90°C in order to remove the excess water. The solution was then again transferred into a preheated muffle furnace maintained at $(550 \pm 10)^\circ\text{C}$. The solution boils foams and ignites to burns with flame; a voluminous, foamy powder was obtained. This entire combustion process was over in about 5 min. The molar ratio and weights of the ingredients used were shown in the Table 1.

The resulting fine powders were calcinated at 750°C for 2h and suddenly cooled to room temperature. Above same process applied for various concentration of Eu^{3+} ($\text{Eu}^{3+} = 0.1, 0.2, 0.5, 1$ and 2%) [12].

Table 1

Molar ratio and weights of the ingredients for $\text{MgY}_{(2-x)}\text{B}_2\text{O}_7 \cdot x\text{Eu}^{3+}$

Compound	Molar Ratio of the Constituents					
$\text{MgY}_2\text{B}_2\text{O}_7 \cdot \text{Eu}^{3+}$	$\text{Mg}(\text{NO}_3)_2$	$\text{Y}(\text{NO}_3)_3$	$\text{Eu}(\text{NO}_3)_3$	H_3BO_3	$\text{CO}(\text{NH}_2)_2$	NH_4NO_3
	1	(2-x)	$x=0.02, 0.01, 0.005, 0.002$ and 0.001	2	6	5.5

$\text{MgY}_{(2-x)}\text{B}_2\text{O}_7 \cdot x\text{Eu}^{3+}$ materials were characterized by using Rigaku Miniflex II X-ray diffractometer with scan speed of 2.000/min and with CuK_α radiation. SEM images are produced on Philips XL 30 SEM system having a resolution of 4.0 nm at 30 kV and 0.5 nm at 1 kV. The PL and PLE spectra are recorded on Hitachi F-7000 fluorescence spectrometer by keeping slit window at 1.0 nm for excitation and emission and PMT voltage at 700V.

3. RESULT AND DISCUSSION

3.1. XRD ANALYSIS OF $\text{MgY}_2\text{B}_2\text{O}_7$

The XRD patterns of $\text{MgY}_{(2-x)}\text{B}_2\text{O}_7 \cdot x\text{Eu}^{3+}$ with different concentrations of activator Eu^{3+} are shown in Figure 1 to verify the phase purity and crystal similarity. The XRD patterns of the $\text{MgY}_{(2-x)}\text{B}_2\text{O}_7 \cdot x\text{Eu}^{3+}$ phosphors have been analyzed for the structure confirmation. As the sample is first time prepared and analyzed careful for peak to peak comparison with the reported compounds, it is found that there was no standard ICDD file available to match the structure of this phosphor. Also, the pattern did not indicate the presence of any phases or peaks from precursor material such as $\text{Y}(\text{NO}_3)_3$, $\text{Mg}(\text{NO}_3)_3$, H_3BO_3 , and other likely phases. This indicates that, all the as-prepared samples were in a similar phase, and the increasing concentration of dopants does not affect the crystal structure of host lattice. So according to the stoichiometric balance calculated using chemical composition of $\text{MgY}_2\text{B}_2\text{O}_7$ we interpreted that the final product was formed in crystalline and homogeneous form called to be $\text{MgY}_2\text{B}_2\text{O}_7$ [13]. This results may indicate that the prepared samples are not the simple chemical mixtures of $\text{Y}(\text{NO}_3)_3$ (2 mole), $\text{Mg}(\text{NO}_3)_3$ (1 mole), H_3BO_3 (2 mole) but a new novel host $\text{MgY}_2\text{B}_2\text{O}_7$ material. Therefore it is indirect evidence for the complete formation of $\text{MgY}_2\text{B}_2\text{O}_7$ compound. Therefore, it might be inferred that our compound has formed in the present phase.

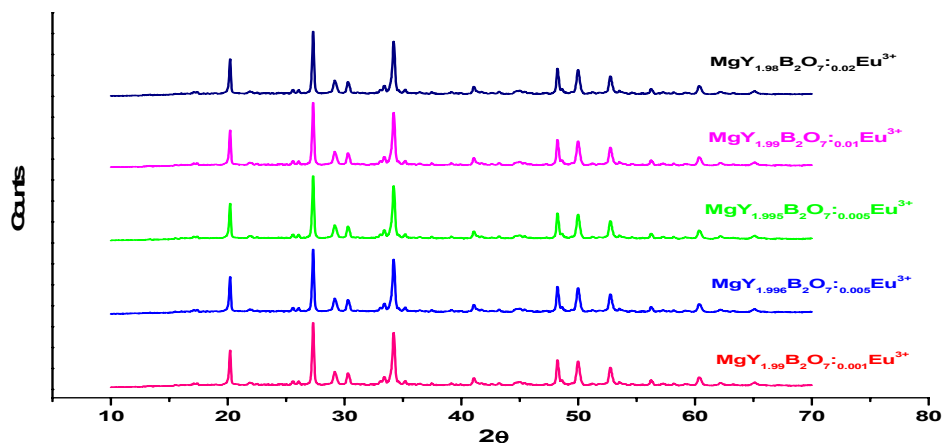


Fig. 1 – XRD pattern of $\text{MgY}_{(2-x)}\text{B}_2\text{O}_7 \cdot x\text{Eu}^{3+}$ ($x = 0.001, 0.002, 0.0005, 0.01$ and 0.02) phosphors.

3.2. SURFACE MORPHOLOGY OF $\text{MgY}_2\text{B}_2\text{O}_7$

SEM images of $\text{MgY}_{1.98}\text{B}_2\text{O}_7 \cdot 0.02\text{Eu}^{3+}$ is represented in Figure 2 synthesized through solution combustion synthesis.

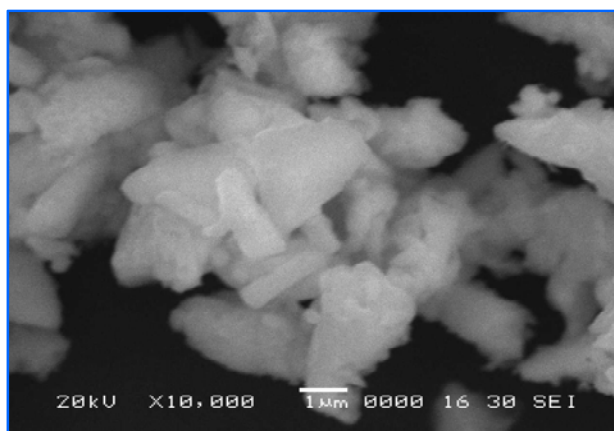


Fig. 2 – SEM image of 0.02 mole Eu^{3+} doped in $\text{MgY}_2\text{B}_2\text{O}_7$.

It indicates that the particles were highly agglomerated crystallites and having irregular surface morphology. The SEM image also reveals the size of particles is in sub micro meter range and was irregular in shape.

3.3. PL PROPERTIES OF $\text{MgY}_{(2-x)}\text{B}_2\text{O}_7:\text{Eu}^{3+}$

Figure 3 shows combined excitation and emission spectra of $\text{MgY}_{1.98}\text{B}_2\text{O}_7:0.02\text{Eu}^{3+}$ phosphor at room temperature. The emission was monitored at 230 nm and excitation was monitored at 613 nm. The excitation spectrum consists of a strong absorption band centered at about 230 nm due to the charge transfer (CT) from the 2p orbital of the O^{2-} ions to the 4f orbital of Eu^{3+} ions. The emission spectra consist of a number of peaks in the range of 500 nm to 550 nm are attributed to ${}^5\text{D}_1$ to ${}^7\text{F}_J$ ($J=0-2$) transition of Eu^{3+} . On the other hand, peaks from 550 nm to 700 nm correspond to ${}^5\text{D}_0$ to ${}^7\text{F}_J$ ($J=0-3$) transition of Eu^{3+} . The main emission at 613 nm was attributed to ${}^5\text{D}_0$ to ${}^7\text{F}_2$ transition of Eu^{3+} ions. It is well known that the relative intensity of the ${}^5\text{D}_0 \rightarrow {}^7\text{F}_1$ and ${}^5\text{D}_0 \rightarrow {}^7\text{F}_2$ transitions strongly depends on the local symmetry of the Eu^{3+} ions [14]. The relative intensity of magnetic dipole transition of ${}^5\text{D}_0 \rightarrow {}^7\text{F}_1$ and the electric dipole transition of ${}^5\text{D}_0 \rightarrow {}^7\text{F}_2$ depended strongly on the symmetry of the crystal lattice around Eu^{3+} . When the Eu^{3+} ions occupy sites with inversion centers, the magnetic dipole transition should be weak, while the electric dipole transition is parity-forbidden and should be relatively strong. The emission spectra of the Eu^{3+} ion doped $\text{MgY}_2\text{B}_2\text{O}_7$ exhibit strong red luminescence corresponding to ${}^5\text{D}_0 \rightarrow {}^7\text{F}_2$ transitions at 613 nm, indicating that the Eu^{3+} ion is located in a non-centrosymmetric position in the host matrix [15]. The result shows that the magnetic dipole transition (${}^5\text{D}_0 \rightarrow {}^7\text{F}_1$) is weaker than the electric dipole transition (${}^5\text{D}_0 \rightarrow {}^7\text{F}_1$).

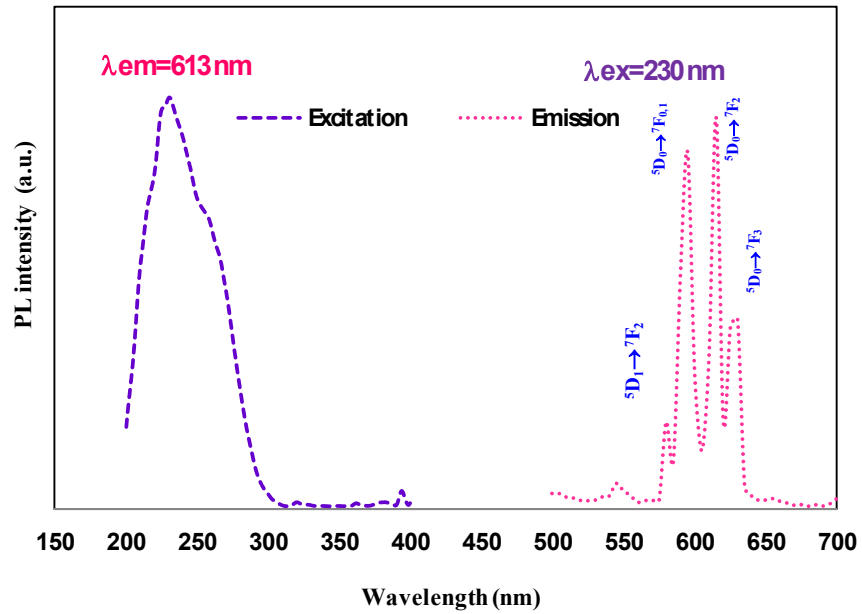


Fig. 3 – Excitation and emission spectra of $\text{MgY}_{1.98}\text{B}_2\text{O}_7:0.02\text{Eu}^{3+}$.

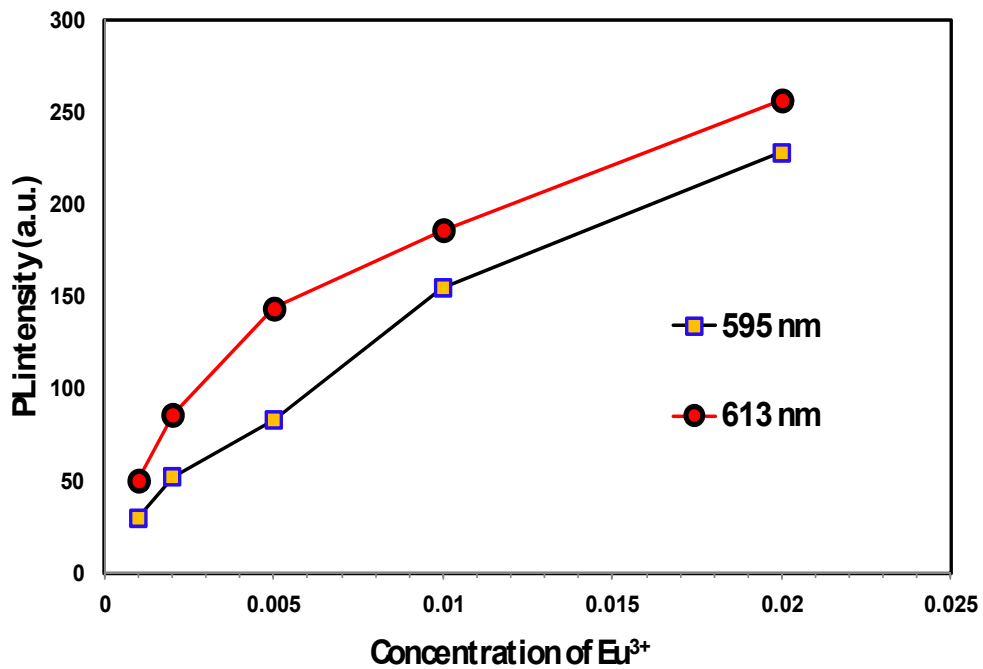


Fig. 4 – PL peak intensity vs concentration of Eu in $\text{MgY}_2\text{B}_2\text{O}_7$ ($\lambda_{ex} = 230\text{ nm}$).

All of the emission spectra exhibit the similar profile with different relative intensities. The emission intensity increases initially with the increase of Eu^{3+} concentration and maximum emission is observed for $x = 0.02$ mole Eu^{3+} doping. Figure 4 represents PL emission intensity at 613 nm and 595 nm of $\text{MgY}_{(2-x)}\text{B}_2\text{O}_7:\text{Eu}^{3+}$ doped with various molar concentration of Eu^{3+} ions ($x = 0.001, 0.002, 0.005, 0.01$ and 0.02). The emission spectra of $\text{MgY}_2\text{B}_2\text{O}_7$ doped with different Eu^{3+} concentrations monitored at 230 nm excitation.

4. COLOUR COORDINATES

Figure 5 presents the CIE 1931 colour space chromaticity diagram to represent the chromaticity of $\text{MgY}_2\text{B}_2\text{O}_7:\text{Eu}^{3+}$ phosphor. The black circle shows their corresponding location of colour coordinates $(x, y) = (0.675, 0.324)$. The red emitting $\text{MgY}_2\text{B}_2\text{O}_7:\text{Eu}^{3+}$ phosphor in the CIE chromaticity diagram as shown in figure 5.

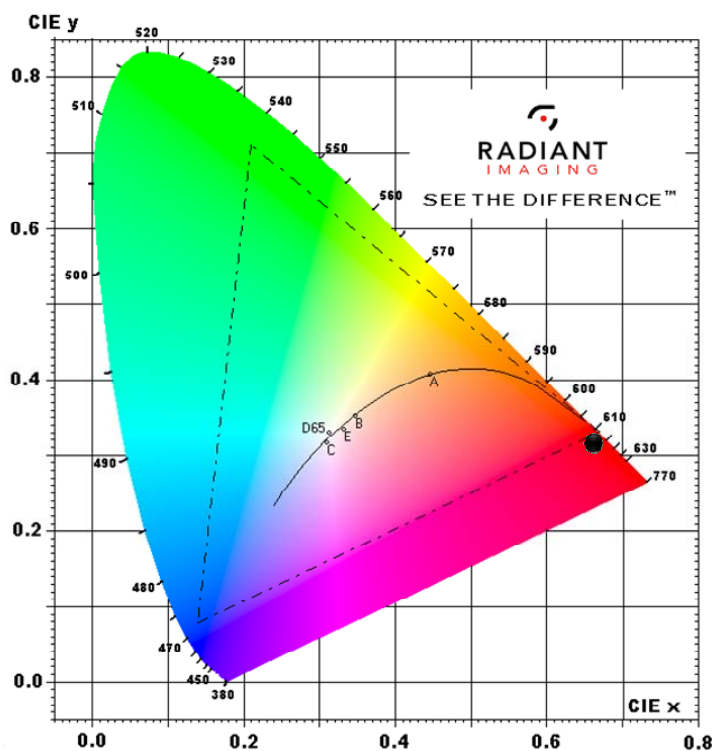


Fig. 5 – CIE colour co-ordinates of $\text{MgY}_2\text{B}_2\text{O}_7:\text{Eu}^{3+}$ phosphor.

5. CONCLUSIONS

The red emitting $\text{MgY}_2\text{B}_2\text{O}_7: \text{Eu}^{3+}$ phosphor was prepared by solution combustion technique. The maximum luminescent intensity of $\text{MgY}_2\text{B}_2\text{O}_7: \text{Eu}^{3+}$ phosphor was observed at 613 nm which is attributed to $^5\text{D}_0 \rightarrow ^7\text{F}_2$ transition. The optimum concentration for Eu^{3+} ions in the given host matrix was found to be 2 mole %. Also there was slightly weak emission observed at 595 nm due to $^5\text{D}_0 \rightarrow ^7\text{F}_1$ transition of Eu^{3+} ions. The PL results indicate that the emission was in the orange-red region of the spectrum. The CIE colour coordinates diagram reveals that the novel $\text{MgY}_2\text{B}_2\text{O}_7: \text{Eu}^{3+}$ phosphor was in the red region and colour coordinates corresponding to the CIE diagram was found to be $x = 0.675$ and $y = 0.324$.

Acknowledgements. One of the authors K. A. Koparkar is thankful to head of the department of physics for providing XRD facility implemented under FIST Program-2010.

REFERENCES

1. D. Wen, J. Shi, Dalton Trans. **42**, 16621-16629 (2013).
2. V. Dubeya, J. Kaur, S. Agrawal, N.S. Suryanarayana, K.V.R. Murthy, Optik, **124**, 5585–5587 (2013).
3. P. A. Nagpure, N. S. Bajaj, R. P. Sonekar, S. K. Omanwar, Ind. J. Pure Appl. Phys. **49**, 799-802 (2011).
4. V. Shivakumar, A. Lakshmanan, R. S. Kumar, S. Kalpana, R. S. Rani, M. T. Jose, Indian Journal of Pure and Applied Physics, **50**, 123-128 (2012).
5. S.R. Anishia, M. T. Jose, O. Annalakshmi, V. Ramasamy, Journal of Luminescence **131**, 2492–2498 (2011).
6. G. Ju, Y. Hu, H. Wu, Z. Yang, C. Fu, Z. Mu, F. Kang, Optical Materials **33**, 1297–1301 (2011).
7. Z. Mu, Y. Hu, L.Chen, X. Wang, Journal of Luminescence **131**, 1687–1691 (2011).
8. R. Balakrishnaiaha, S. S. Yi, K. Jang, H. S. Lee, B. K. Moon, J. H. Jeong, Materials Research Bulletin, 46, 621–626 (2011).
9. B. Yang, Z. Yang, Y. Liu, F. Lu, P. Li, Y. Yang, X. Li, Ceramics International **38**, 4895–4900 (2012).
10. K. A. Koparkar, N. S. Bajaj, S. K. Omanwar, Indian Journal of Physics, **80**, 10.1007/s12648-014-0554-y.
11. N. S. Bajaj, S. K. Omanwar, Opt. Mat. **35**, 1222-1225 (2013).
12. N. S. Bajaj, S. K. Omanwar, J. Rare Earths **30**, 1005-1008 (2012).
13. K. A. Koparkar, N. S. Bajaj, S. K. Omanwar, Advances in Optical Technologies, ID **706459**, 1-5 (2014).
14. R. H. Krishna, B. M. Nagabhushana, H. Nagabhushana, N. Suriya Murthy, S. C. Sharma, C. Shivakumara, R. P. S. Chakradhar, J. Phys. Chem. C **117**, 1915–1924 (2013).
15. L. Wang, Y. Wang, Materials Science and Engineering B **139**, 232–234 (2007).